POLITECNICO DI TORINO
Repository ISTITUZIONALE

Record-Low 1/f Noise at 4 K in Cryogenic InGaAs HEMTs for Quantum Computing via Quantum Well Heterostructure Engineering

Original
Record-Low 1/f Noise at 4 K in Cryogenic InGaAs HEMTs for Quantum Computing via Quantum Well Heterostructure Engineering / Jeong, J., Cha, E., Tugnoli, S., Olziersky, A., Caimi, D., Sousa, M., Reidt, S., Gotsmann, B., Kim, S., Zota, C.. - (2026). (2026 IEEE International Electron Devices Meeting (IEDM)).

Availability:
This version is available at: 11583/3017733 since: 2026-11-10T11:05:50Z

Publisher:
IEEE

Published
DOI:

Terms of use:

This article is made available under terms and conditions as specified in the corresponding bibliographic description in the repository

Publisher copyright
IEEE postprint/Author's Accepted Manuscript

©2026 IEEE. Personal use of this material is permitted. Permission from IEEE must be obtained for all other uses, in any current or future media, including reprinting/republishing this material for advertising or promotional purposes, creating new collecting works, for resale or lists, or reuse of any copyrighted component of this work in other works.

(Article begins on next page)

18 November 2026

Record-Low 1/f Noise at 4 K in Cryogenic InGaAs HEMTs for Quantum Computing via Quantum Well Heterostructure Engineering

Jaeyong Jeong[1,2,3,4,*], Eunjung Cha[1,5], Sofia Tugnoli[1], Antonis Olziersky[1], Daniele Caimi[1], Marilyne Sousa[1], Steffen Reidt[1], Bernd Gotsmann[1], Sanghyeon Kim[2,†] and Cezar Zota[1,‡]

[1]IBM Research Europe, Rueschlikon, Switzerland, [2]School of Electrical Engineering, KAIST, Korea,
[3]Department of Electrical Engineering, UNIST, Korea, [4]School of Semiconductor Materials and Devices Engineering, UNIST, Korea,
[5]Paul Scherrer Institute, Villigen, Switzerland
[*]E-mail: jaeyong.jeong@unist.ac.kr, [†]E-mail: shkim.ee@kaist.ac.kr, [‡]E-mail: zot@zurich.ibm.com

***Abstract*—**In this work, we report the first systematic study of low-frequency 1/f noise (LFN) at 4 K in cryogenic InGaAs HEMTs used in quantum computing low-noise amplifiers and interfaces. We show how the quantum well heterostructure can be engineered to suppress cryogenic LFN, and demonstrate the lowest ever reported transistor LFN at 4 K. LFN in cryogenic transistors is a key bottleneck for quantum computing as it degrades the signal-to-noise ratio of readout amplifiers and phase/frequency noise in control lines, reducing qubit coherence and readout fidelity. In contrast to other metrics, LFN performance tends to degrade from 300 to 4 K. Here, we show non-monotonic 1/f noise *T*-dependence with a minimum at 200 K, indicating additional disorder-induced noise mechanisms beyond the carrier number fluctuation model at 4 K. By comparing several quantum well designs, we identify channel-barrier interface disorder as the dominant origin of excess cryogenic LFN, and show that heterostructure engineering can suppress 4 K 1/f noise by two orders of magnitude. The resulting HEMTs show a combination of both record lowest reported noise indication factor, 0.14 $\sqrt{\text{V·mm/S}}$, and flat band voltage noise < $1\text{x}10^{-12}$ V^2/Hz.

I. Introduction

The development of quantum computers over the next years will require many improvements to the supporting cryogenic electronic infrastructure. A widely considered cryogenic electronics architecture places control and readout electronics close to the qubit chip in order to reduce the number and length of wires in the cryostat (**Fig. 1(a)**). InGaAs HEMTs are promising devices for such cryogenic electronics since they combine high electron mobility, large microwave gain, and low-noise operation at cryogenic temperatures, making them attractive for readout low-noise amplifiers (LNAs) [1-4], in which they are already standard industrial technology, and various novel signal routing circuits [5-7].

Despite major progress in DC and RF performance, a comprehensive understanding of the role of disorder in cryogenic HEMTs is lacking. As thermally activated carrier transport is suppressed at 4 K, disorder-related effects that are negligible at room temperature can become dominant, causing subthreshold swing saturation, threshold-voltage instability, random telegraph noise, and excess low-frequency noise (LFN) [8-12]. Although anomalous cryogenic LFN enhancement has been reported in Si MOSFETs (**Fig. 1(b)**), systematic studies on disorder-induced LFN in InGaAs HEMTs are still missing. While superconducting qubits operate at GHz frequencies where LFN is negligible, LFN gets upconverted into close-in phase noise on microwave control and readout tones, as well as causes slow drift of bias points, gains, and phases, which degrades e.g. readout discrimination, calibration stability and multiplexing performance. An improved understanding of cryogenic LFN and its mitigation strategies is thus important.

In this work, we present the first systematic analysis of cryogenic LFN in InGaAs HEMTs down to 4 K. The key contributions of this work are: (i) systematic characterization of disorder-induced LFN in InGaAs HEMTs from 300 K to 4 K, (ii) experimental observation of non-monotonic temperature-dependent LFN, (iii) identification of the dominant physical origin of excess cryogenic LFN through structural comparison, and (iv) demonstration of a channel-engineering strategy to suppress disorder-induced noise. These findings provide fundamental insights into disorder in cryogenic InGaAs HEMTs and offer a path toward ultra-low-power, low-noise cryogenic electronics for future quantum computing systems.

II. Device Design and Fabrication

A. III-V heterostructure design

Fig. 2 illustrates the possible LFN sources in an InGaAs HEMT: (1) channel roughness and (2) channel/barrier-interface disorder, (3) traps inside the InAlAs barrier, and (4) surface-related traps above the barrier. To distinguish these contributions, two series of HEMTs were fabricated with different heterostructure designs (**Fig. 3**). In the channel series, a 15-nm $In_{0.65}Ga_{0.35}As$ single channel, a 9-nm $In_{0.75}Ga_{0.25}As$ single channel, and a $In_{0.53}Ga_{0.47}As/In_{0.80}Ga_{0.20}As/In_{0.53}Ga_{0.47}As$ composite channel were compared at a fixed 4-nm InAlAs barrier. Here, the main difference in disorder sources are (1) and (2), as these channel layers have different lattice mismatch. In the barrier series, the $In_{0.75}Ga_{0.25}As$ channel was fixed while the InAlAs barrier thickness was 3, 4 and 5 nm, which should modulate disorder sources (3) and (4). In both these series, the remaining epitaxial layers, including the InP etch stop and InAlAs spacer, were kept identical.

B. Fabrication of cryogenic InGaAs HEMTs

InGaAs HEMT heterostructures were epitaxially grown on InP substrates by molecular beam epitaxy (MBE), with variations in channel design and barrier thickness as stated above. The devices were fabricated using a T-gate process flow adapted from [4], featuring 100-nm gate lengths and non-alloyed ohmic contacts to ensure low contact resistance and excellent thermal stability. Devices are encapsulated in 20 nm Al_2O_3 which passivates the exposed recess-etched surfaces at either side of the gate. A cross-sectional STEM image of a fabricated InGaAs HEMT is shown in **Fig. 2(b)** and **(c)**, highlighting the III–V heterostructure and the gate stack.

III. Results and Discussion

A. DC and RF characteristics of cryogenic InGaAs HEMTs

Fig. 4–7 summarize the temperature-dependent DC characteristics of a device with an $In_{0.75}Ga_{0.25}As$ channel and a 4-nm-thick barrier. Cooling from 300 K to 4 K improves transfer characteristics and increases g_m because of enhanced mobility and reduced parasitic resistance (**Fig. 4** and **5**) [3]. These improvements

are also reflected in the output characteristics, with the device exhibiting R_{on} of 268 Ω·mm at 4 K. The SS–I_D characteristics systematically improve with decreasing temperature (**Fig. 6**), and the minimum SS follows the thermal limit over a wide temperature range before saturating at 4.8 mV/dec at 4 K (**Fig. 7**). This is among the lowest reported SS for a cryogenic InGaAs HEMT to date.

The heterostructure design series maintain strong cryogenic device performance. At 4 K, the peak g_m ranges from ~1.8 to 2.3 S/mm, with the composite channel showing the highest value due to the high mobility of the $In_{0.80}Ga_{0.20}As$ central layer (**Fig. 8(a)**). A key figure-of-merit for cryogenic LNAs is the noise indication factor $\sqrt{I_D}/g_m$, which should be minimized. It is derived from the Pospieszalski noise model, a widely used equivalent-circuit thermal noise model for the minimum noise temperature, T_{min}, in microwave FETs [1]. The measured $\sqrt{I_D}/g_m$ reaches 0.14 $\sqrt{\text{V·mm/S}}$ for the optimized barrier design, and remains low for the composite channel (**Fig. 8(b)**). The 4 K RF gain in **Fig. 9** yields f_T = 552 GHz and f_{MAX} = 472 GHz, confirming excellent gain levels for cryogenic LNAs operating at typical qubit frequencies. Benchmarking in **Fig. 10** shows that 3 nm barrier devices achieve a record-low noise indication factor for cryogenic III-V HEMTs.

B. Temperature- and bias-dependent LFN

The cryogenic LFN characteristic of an $In_{0.75}Ga_{0.25}As$-channel HEMT with a 4-nm-thick barrier is shown in **Fig. 11-15**. The drain-current transients at equal overdrive show visibly larger fluctuations at 4 K than at 300 K (**Fig. 11**). Consistently, the normalized drain-current noise, S_{ID}/I_D^2, at V_{OV} = 0 V is enhanced across the measured frequency range at 4 K (**Fig. 12**). Bias-dependent spectra in **Fig. 13** exhibit approximately 1/f behavior at both temperatures, with stronger noise and bias dependence at 4 K. The normalized noise measured at 10 Hz first decreases as the device is cooled, but then rises again at cryogenic temperature (**Fig. 14**), demonstrating that the low-temperature noise cannot be inferred by a simple extrapolation from room temperature.

To determine the dominant electrical LFN mechanism, S_{ID}/I_D^2 was compared with the carrier number fluctuation (CNF) and carrier mobility fluctuation (CMF) dependencies. The measured data closely follow $(g_m/I_D)^2$ at both 300 K and 4 K (**Fig. 15**), whereas the mobility-fluctuation form does not reproduce the bias dependence. The noise can thus be expressed as $S_{ID}/I_D^2 = (g_m/I_D)^2 \times S_{vfb}$, where S_{vfb} is the equivalent flat-band-voltage noise spectral density. Therefore, to accurately evaluate and compare the intrinsic noise characteristics of the devices S_{vfb} should be extracted based on this CNF model.

C. Physical origin of excess noise in cryogenic InGaAs HEMTs

Fig. 16 shows the extracted S_{vfb} as a function of temperature for an $In_{0.75}Ga_{0.25}As$/4 nm barrier device. As the temperature decreases, S_{vfb} initially decreases but starts to increase again below ~200 K. This behavior cannot be fully explained by the conventional CNF model. In the CNF model, the trap density (N_t) is generally treated as a nearly temperature-independent parameter. Therefore, as the temperature decreases, the reduced k_BT and suppressed thermal activation is expected to decrease the noise level. However, the experimentally observed non-monotonic temperature dependence suggests the presence of at least two competing low-frequency noise contributions with different activation energies and/or spatial origins, rather than a single monotonic trap freeze-out process. The presence of a crossover temperature is consistent with a broad distribution of traps whose switching rates $\Gamma \propto \exp(-E_a/k_BT)$ shift out of the measurement window as T is lowered, while a separate set of slower traps remain active at 4 K. Possible microscopic locations of disorder are summarized in **Fig. 17**. To identify the origin of the cryogenic excess noise, we compared the LFN characteristics of the two heterostructure design device series.

The barrier-thickness series examines whether traps in the InAlAs barrier or at the upper surface dominate this excess noise. Despite changing the barrier thickness from 5 to 3 nm, the devices show nearly overlapping S_{ID}/I_D^2–I_D characteristics and only a small variation in extracted S_{vfb} around $5{\cdot}10^{-11}$ V²/Hz at 4 K (**Fig. 18**). Barrier and surface traps, which should show a reduced response for thicker barriers, therefore cannot account for the large cryogenic noise enhancement. In contrast, the channel series exhibits a pronounced and systematic change in noise (**Fig. 19**). Reducing the In content from 0.75 to 0.65 lowers S_{vfb} by more than one order of magnitude, consistent with reduced lattice mismatch and interface roughness. The composite $In_{0.53}Ga_{0.47}As/In_{0.80}Ga_{0.20}As/In_{0.53}Ga_{0.47}As$ channel further suppresses S_{vfb} to the 10^{-13} V²/Hz range. The lattice-matched $In_{0.53}Ga_{0.47}As$ outer layers form improved interfaces with $In_{0.52}Al_{0.48}As$, while the central $In_{0.80}Ga_{0.20}As$ layer retains high electron mobility. The temperature-dependent comparison in **Fig. 20** confirms that this channel-structure dependence persists throughout the cryogenic regime. Together with the weak barrier-thickness dependence, these results identify channel/barrier-interface disorder as the primary origin of cryogenic excess LFN in InGaAs HEMTs.

Fig. 21(a) summarizes the results on cryogenic LFN mitigation using heterostructure engineering in this work. The relevant traps are interface traps and defects associated with misfit dislocations and local alloy disorder at the channel/barrier interface. Because these defects are structurally pinned by the epitaxial/lattice mismatch properties, their switching dynamics are only weakly thermally activated at low temperature, leading to a broad, slowly varying distribution of time constants that results in excess LFN down to 4 K. The composite channel implements lattice-matched $In_{0.53}Ga_{0.47}As$ and an ultra-thin high-mobility central channel which significantly reduces these defects. **Fig. 21(b)** benchmarks the LFN performance of our devices against state-of-the-art cryogenic CMOS and HEMTs [10, 11, 13]. Our composite $In_{0.80}Ga_{0.20}As$ channel devices achieve one order of magnitude lower LFN, ~$5{\cdot}10^{-13}$ V²/Hz, than previously reported and thus the record-lowest LFN at 4 K to date.

IV. Conclusions

We present the first systematic study of cryogenic 1/f noise in InGaAs HEMTs. The extracted flat band voltage noise shows an upturn at low temperature, indicating excess LFN at 4 K. Comparison of several quantum well heterostructure variations show that cryogenic noise is only weakly affected by the barrier geometry but strongly depends on the channel configuration, which highlights channel/barrier-interface disorder due to lattice mismatch as the dominant noise source. Through a composite tri-layer quantum well design, interfacial disorder is substantially suppressed while strong DC performance is preserved, resulting in both record-low 1/f noise and noise indication factor, $5{\cdot}10^{-13}$ V²/Hz and 0.14 $\sqrt{\text{V·mm/S}}$, respectively. These results establish channel-interface disorder control as a key design guideline for future quantum computer electronics such as cryogenic LNAs.

Acknowledgment

This work was supported by NCCR SPIN, a National Centre of Competence in Research, funded by the Swiss National Science Foundation (grant number 51NF40-180604), by the SNSF projects IZKSZ2_218591, by the BRNC and by National Research Foundation of Korea (NRF) grant (No. RS-2026-25489040, RS-2026-25578911, RS-2023-00224408, RS-2024-00400931).

Motivation: Understanding poorly understood cryogenic disorder characteristics and mechanisms in InGaAs HEMTs

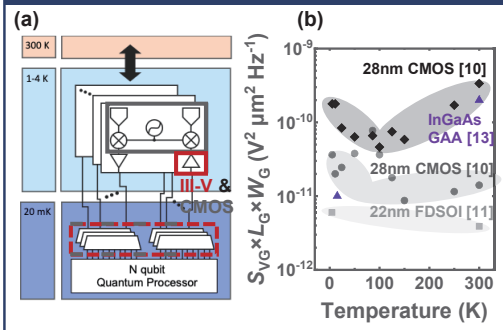
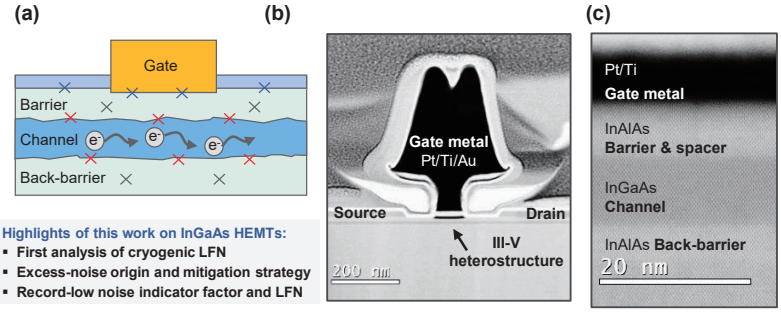


Fig. 1. (a) Schematic of a large-scale quantum computing system. InGaAs HEMTs are promising for cryogenic LNAs and routing circuits; however, a systematic understanding and mitigation of cryogenic device disorder, which limits their performance, remains essential. (b) Cryogenic LFN benchmark across divers FET technologies, showing excess noise in cryogenic CMOS and emphasizing the need for systematic analysis in III–V-based cryogenic devices



Highlights of this work on InGaAs HEMTs:
- First analysis of cryogenic LFN
- Excess-noise origin and mitigation strategy
- Record-low noise indicator factor and LFN

Fig. 2. (a) Schematic cross-section of an InGaAs HEMT illustrating possible cryogenic low-frequency-noise sources in the barrier, channel, and back-barrier regions. This work systematically identifies the dominant noise origin and develops a channel-engineering strategy to suppress cryogenic excess noise. (b) Cross-sectional TEM image of the fabricated InGaAs HEMT, showing the source, drain, gate metal, and channel. (c) Enlarged TEM image of the gate stack, consisting of a Pt/Ti gate, a InAlAs barrier/spacer, a InGaAs channel, and an InAlAs back-barrier.

Device Design and Fabrication of InGaAs HEMT

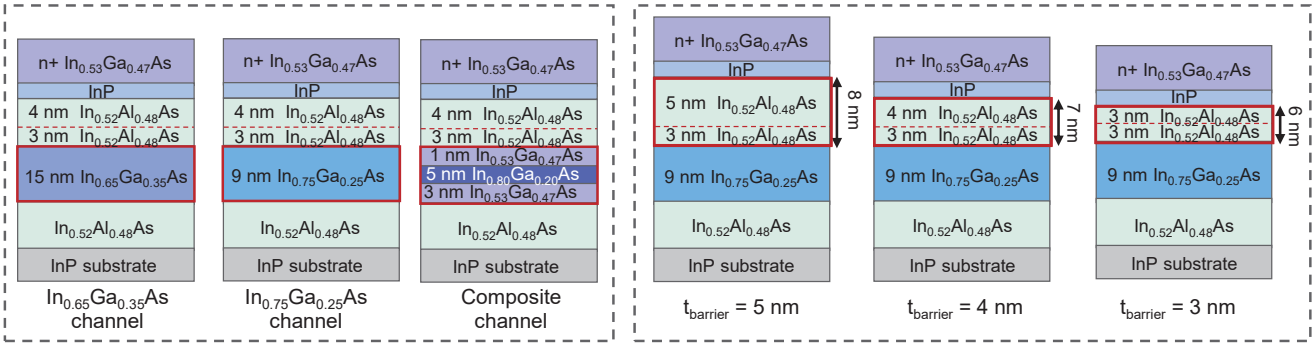


Fig. 3. Epitaxial layer designs used to investigate the effects of the channel and barrier structures on the cryogenic device characteristics. The channel design was varied from a composite quantum-well structure to single InGaAs channels with different In compositions and three barrier-thickness splits with 3, 4, and 5 nm $In_{0.52}Al_{0.48}As$ barriers, while the 3-nm InAlAs spacer was kept fixed.

Temperature-Dependent DC Characteristics of InGaAs HEMTs

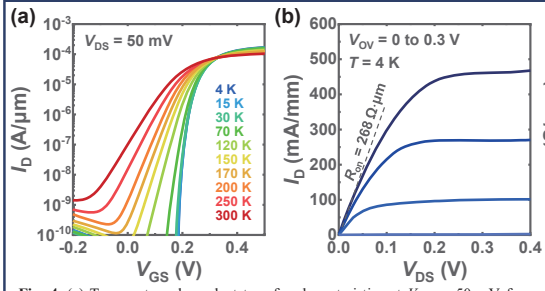


Fig. 4. (a) Temperature-dependent transfer characteristics at V_{DS} = 50 mV from 300 K to 4 K and (b) output characteristics at 4 K of the InGaAs HEMT. The device shows a clear and systematic temperature dependence, with improved switching characteristics at cryogenic temperature. At 4 K, the cryogenic InGaAs HEMT achieves an on-resistance, R_{on}, 268 Ω·mm.

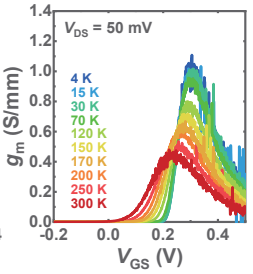


Fig. 5. (a) Transconductance (g_m) as a function of V_{GS} at V_{DS} = 50 mV. The device shows enhanced gm at low temperature, exceeding 1 S/mm at 4K even at a drain bias of only 50 mV.

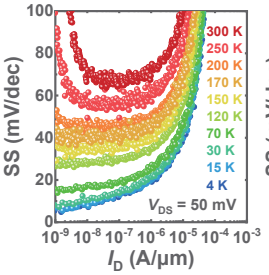


Fig. 6. (a) Subthreshold swing (SS) plotted as a function of drain current (I_D) for different temperatures, measured at V_{DS} = 50 mV.

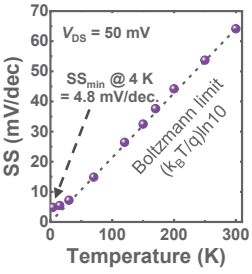


Fig. 7. Subthreshold swing as a function of temperature. The extracted SS follows the Boltzmann limit over a wide temperature range and reaches 4.8 mV/dec ac 4 K, highlighting the steep subthreshold switching of the device at cryogenic temperature.

Heterostructure-dependent DC and RF properties

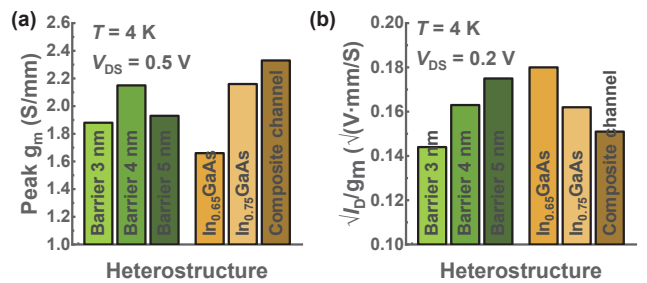


Fig. 8. Comparison of the (a) peak transconductance, $g_{m,peak}$, at V_{DS} = 0.5 V and (b) noise indication factor ($\sqrt{I_D}/g_m$), at V_{DS} = 0.2 V for InGaAs HEMTs with different barrier thicknesses and channel configurations at 4 K.

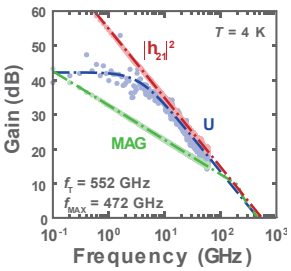


Fig. 9. RF gain characteristics of the InGaAs HEMTs measured at 4 K. The device exhibits f_T and f_{MAX} of 552 and 472 GHz at 4 K.

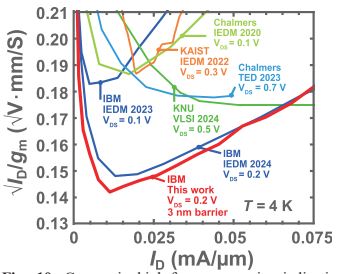


Fig. 10. Cryogenic high-frequency noise indication factor versus drain current to compare with state-of-the-art InGaAs HEMTs. This work demonstrates improved noise indication factor with performance optimized for low-power cryogenic electronics.

Temperature- and Bias-Dependent Low frequency Noise Characteristics

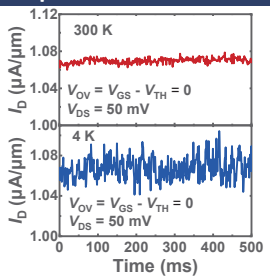


Fig. 11. Drain-current transients of InGaAs HEMTs measured at 300 and 4 K. V_{TH} was independently extracted at each temperature at I_D = 1 μA/μm. Enhanced current fluctuations at 4 K indicate increased cryogenic low-frequency noise.

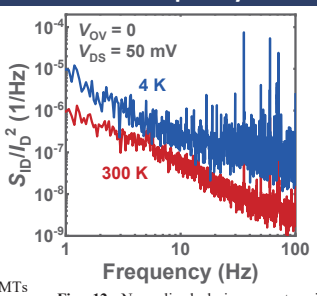


Fig. 12. Normalized drain current noise, S_{ID}/I_D^2, as a function of frequency at 300 K and 4 K for V_{ov} = 0 V and V_{DS} = 50 mV.

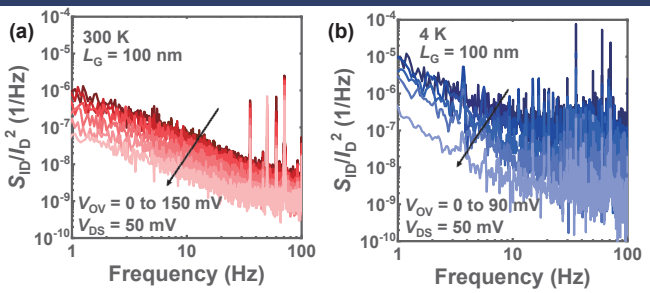


Fig. 13. S_{ID}/I_D^2 of InGaAs HEMT for V_{DS} = 50 mV under different V_{GS} biases at (a) 300 K and (b) 4 K. Both 300 K and 4 K measurements show clear low-frequency noise behavior, while the 4 K spectra exhibit enhanced noise levels and stronger bias dependence.

Origin of Excess Noise of Cryogenic InGaAs HEMT

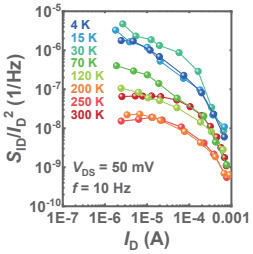


Fig. 14. Temperature-dependent LFN characteristics of InGaAs HEMTs. The noise is reduced upon cooling, followed by an upturn at cryogenic temperatures.

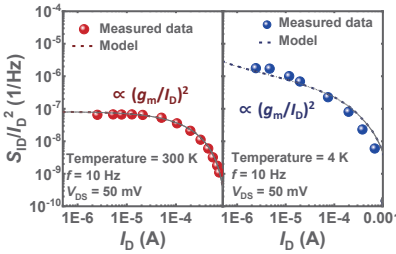
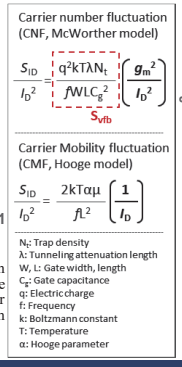


Fig. 15. Normalized drain current noise, S_{ID}/I_D^2, as a function of I_D measured at 300 K and 4 K. At all temperature, the noise follows $(g_m/I_D)^2$, indicating that carrier number fluctuation is the dominant low frequency noise mechanism of cryogenic InGaAs HEMTs



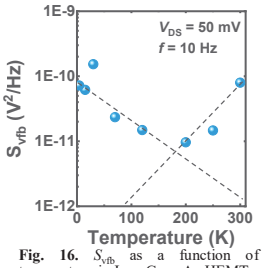


Fig. 16. S_{vfb} as a function of temperature in $In_{0.75}Ga_{0.25}As$ HEMTs. The noise initially decreases with cooling, followed by an upturn at cryogenic temperatures, indicating disorder-related excess noise under cryogenic operation.

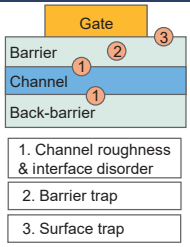
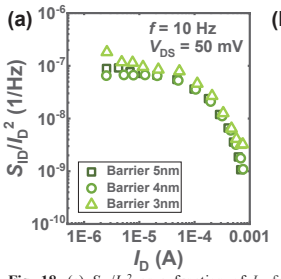


Fig. 17. Schematic illustration of possible disorder sources in InGaAs HEMTs responsible for cryogenic excess noise. Barrier-thickness and channel-structure splits enable identification of the dominant disorder source.

Mitigation Strategy for Reducing Cryogenic Excess Noise in InGaAs HEMTs



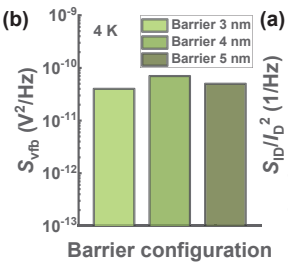
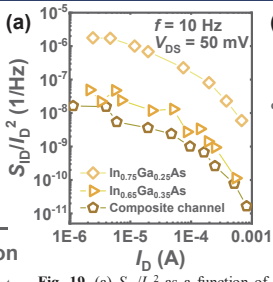


Fig. 18. (a) S_{ID}/I_D^2 as a function of I_D for $In_{0.75}Ga_{0.25}As$ HEMTs with different barrier thickness. The noise was measured at f = 10 Hz and V_{DS} = 50 mV. (b) S_{vfb} extracted at f = 10 Hz for different barrier thicknesses. S_{vfb} shows little dependence on barrier thickness, indicating that barrier traps and surface traps are not the dominant sources of disorder-related excess noise at cryogenic temperatures.



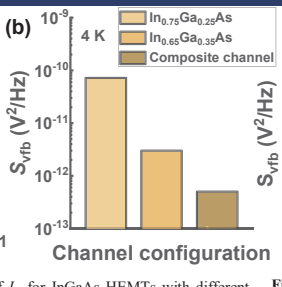


Fig. 19. (a) S_{ID}/I_D^2 as a function of I_D for InGaAs HEMTs with different channel configurations and a fixed 4-nm-thick barrier, measured at f = 10 Hz and V_{DS} = 50 mV. (b) Extracted S_{vfb} at f = 10 Hz for each channel configuration. The S_{vfb} decreases as the In composition in the channel is reduced, and the lattice-matched $In_{0.53}Ga_{0.47}As/In_{0.8}Ga_{0.2}As/In_{0.53}Ga_{0.47}As$ composite channel exhibits the lowest S_{vfb}, indicating suppressed channel/interface-related noise.

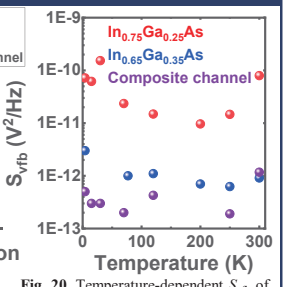


Fig. 20. Temperature-dependent S_{vfb} of InGaAs HEMT with different channel structures. A strong dependence on channel structure is observed, indicating that channel roughness and interface disorder are the primary origins of the excess noise.

Summary & Benchmark

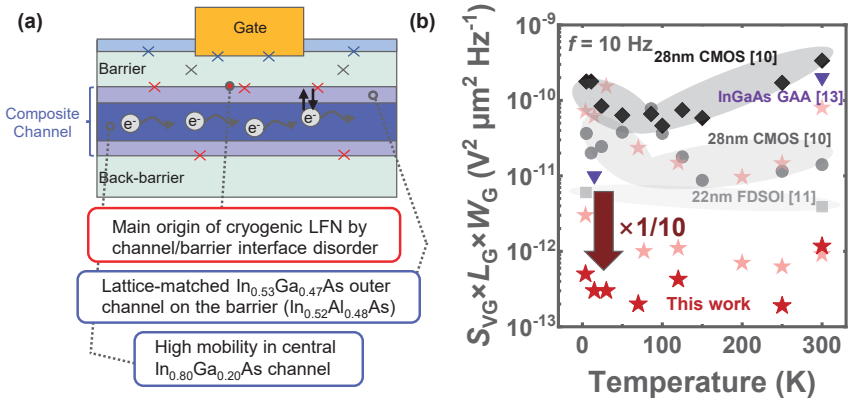


Fig. 21. (a) Summary of this work showing that cryogenic low-frequency noise primarily originates from channel/barrier interface disorder. The composite InGaAs quantum-well channel mitigates interface disorder using lattice-matched $In_{0.53}Ga_{0.47}As$ outer channels while preserving high mobility in the central $In_{0.8}Ga_{0.2}As$ channel. (b) Benchmarking of the normalized noise metric, $S_{vfb} \times L_G \times W_G$, against state-of-the-art cryogenic transistors [10, 11, 13]. This work achieves more than one order of magnitude lower noise at cryogenic temperatures, demonstrating the effectiveness of channel/interface engineering for low-noise quantum computing electronics.

References

[1] M.W.Pospieszalski, *IEEE TMTT*, 37, p.1340 (1989), doi: 10.1109/22.32217.
[2] J. Grahn et al., *IEDM*, p. 541 (2020), doi: 10.1109/IEDM13553.2020.9372031.
[3] J. Jeong *et al.*, *Symp. on VLSI*, p. 328 (2021), doi: 10.1109/VLSITechnologyandCir46769.2022.9830449.
[4] E. Cha *et al.*, *IEDM*, p. 1 (2024), doi: 10.1109/IEDM50854.2024.10873434.
[5] J. Jeong *et al.*, *Nature Communications*, 15, p. 10809 (2024), doi: 10.1038/s41467-024-55077-1.
[6] A. Ferraris et al., *IEDM*, p. 4.6.1 (2022), doi: 10.1109/IEDM45625.2022.10019536.
[7] J. Jeong *et al.*, *IEDM*, p. 4.5.1 (2022), doi: 10.1109/IEDM 45625.2022.10019363.
[8] Q.-T. Zhao *et al.*, *Nature Reviews Electrical Engineering*, 2, p.227 (2025), doi: 10.1038/s44287-025-00157-7.
[9] A. Beckers *et al.*, *IEEE EDL*, 41, p. 276 (2020), doi: 10.1109/LED.2019.2963379.
[10] R. Asanovski *et al.*, *IEDM*, p. 1 (2022), doi: 10.1109/IEDM45625.2022.10019388.
[11] P. B. Paz *et al.*, *IEEE TED*, 67, p. 4563 (2020), doi: 10.1109/TED.2020.3021999.
[12] H. Oka *et al.*, *Symp. on VLSI*, p. 1 (2020), doi: 10.1109/VLSITechnology18217.2020.9265013.
[13] M. S. Ram *et al.*, *IEEE EDL*, 43, p. 2033 (2022), doi: 10.1109/LED.2022.3216022.